BBA - Bioenergetics 1861 (2020) 148133

Contents lists available at ScienceDirect

BBA - Bioenergetics

journal homepage: www.elsevier.com/locate/bbabio

Fine-tuning of the respiratory complexes stability and supercomplexes assembly in cells defective of complex III

Concetta V. Tropeano[a], Serena J. Aleo[a], Claudia Zanna[a], Marina Roberti[b], Letizia Scandiffio[b], Paola Loguercio Polosa[b], Jessica Fiori[c], Emanuele Porru[c], Aldo Roda[c], Valerio Carelli[d,e], Stefan Steimle[f], Fevzi Daldal[f], Michela Rugolo[a,*], Anna Ghelli[a,*]

[a] Dipartimento di Farmacia e Biotecnologie (FABIT), Università di Bologna, Bologna, Italy
[b] Dipartmento di Bioscienze, Biotecnologie e Biofarmaceutica, Università di Bari, Italy
[c] Dipartimento di Chimica "Giacomo Ciamician", Università di Bologna, Bologna, Italy
[d] Dipartimento di Scienze Biomediche e Neuromotorie (DIBINEM), Università di Bologna, Bologna, Italy
[e] IRCCS Istituto delle Scienze Neurologiche di Bologna, Ospedale Bellaria, Bologna, Italy
[f] Department of Biology, University of Pennsylvania, Philadelphia, PA 19104, USA

ARTICLE INFO

Keywords:
Respiratory chain supercomplexes
MT-CYB gene in-frame microdeletion
Cytochrome *b* depletion complex III dysfunction
N-acetylcysteine, rotenone

ABSTRACT

The respiratory complexes are organized in supramolecular assemblies called supercomplexes thought to optimize cellular metabolism under physiological and pathological conditions. In this study, we used genetically and biochemically well characterized cells bearing the pathogenic microdeletion m.15,649–15,666 (ΔI300-P305) in *MT-CYB* gene, to investigate the effects of an assembly-hampered CIII on the re-organization of supercomplexes. First, we found that this mutation also affects the stability of both CI and CIV, and evidences the occurrence of a preferential structural interaction between CI and $CIII_2$, yielding a small amount of active CI + $CIII_2$ supercomplex. Indeed, a residual CI + CIII combined redox activity, and a low but detectable ATP synthesis driven by CI substrates are detectable, suggesting that the assembly of CIII into the CI + $CIII_2$ supercomplex mitigates the detrimental effects of *MT-CYB* deletion. Second, measurements of oxygen consumption and ATP synthesis driven by NADH-linked and $FADH_2$-linked substrates alone, or in combination, indicate a common ubiquinone pool for the two respiratory pathways. Finally, we report that prolonged incubation with rotenone enhances the amount of CI and $CIII_2$, but reduces CIV assembly. Conversely, the antioxidant *N*-acetylcysteine increases $CIII_2$ and CIV_2 and partially restores respirasome formation. Accordingly, after NAC treatment, the rate of ATP synthesis increases by two-fold compared with untreated cell, while the succinate level, which is enhanced by the homoplasmic mutation, markedly decreases. Overall, our findings show that fine-tuning the supercomplexes stability improves the energetic efficiency of cells with the *MT-CYB* microdeletion.

1. Introduction

The respiratory electron transport in the mitochondrial inner membrane occurs through four oligomeric enzyme complexes, referred to as complexes I, II, III and IV (CI, CII, CIII and CIV), which are connected by two mobile redox carriers, the lipophilic quinone (CoQ) within the lipid bilayer, and the hydrophilic protein cytochrome *c*, associated with the outer surface of the inner membrane [1]. It is becoming increasingly clear that the respiratory complexes can coexist in mitochondrial membrane as single functional entities CI, CII, dimer of CIII ($CIII_2$) and CIV, and also as supramolecular assemblies, called supercomplexes (SCs) (for recent reviews see [2,3]). In SCs, the three proton pumping units of respiratory chain (CI, $CIII_2$ and CIV) are associated with different composition and stoichiometry. In mammalian mitochondria, CI could interact with $CIII_2$ and one or more CIV monomers to form the so-called respirasome (CI + $CIII_2$ + CIV_n) that is present together with other SCs containing CI + $CIII_2$ or $CIII_2$ + CIV [2].

The structural and functional significance of SCs is still under intense debate. In particular, the SCs role in regulating the overall activity of the respiratory chain, in protecting against ROS production, and in stabilizing the assembled respiratory complexes remains unsolved [2–5]. Clearly, the structural architecture of SCs has important implications in human mitochondrial diseases. The first extensive analysis of the state of SCs in patients with isolated deficiency of single

* Corresponding authors.
E-mail addresses: michela.rugolo@unibo.it (M. Rugolo), annamaria.ghelli@unibo.it (A. Ghelli).

https://doi.org/10.1016/j.bbabio.2019.148133
Received 31 January 2019; Received in revised form 11 November 2019; Accepted 5 December 2019
Available online 09 December 2019
0005-2728/

complexes revealed that mutations inducing CIII disassembly caused the complete loss of the respirasome and CI instability [6]. Several lines of evidence indicate that alterations of individual CIII or CIV assembly also induce concomitant CI dysfunction, suggesting that the formation of SCs is also important for the stability of CI [6–13]. In any event, it is clear that the functional alterations of CI, induced by CIII deficiencies, become clear only when CIII is partially or completely disassembled, but not when it is assembled despite having reduced enzymatic activities [14]. It has been proposed that the amount of respirasome could be regulated by the quinone pool redox state, i.e. the $CoQH_2/CoQ$ ratio in the membrane. Guaras et al., reported that deficiencies in respiratory complexes causing increased $CoQH_2/CoQ$ ratio could induce reverse electron transport (RET) from $CoQH_2$ to CI [15]. Consequently, CI-dependent production of superoxide could be enhanced, causing the oxidation of critical cysteine residues of CI, increasing its instability and triggering its degradation. Accordingly, the CoQ redox state has been proposed to act as a metabolic sensor, allowing cells to finely-tune the amount of CI associated with the respirasomes versus the amounts of free $CIII_2$ or $CIII_2$ + CIV to optimize the respiratory chain efficiency [15].

The coexistence of both SCs and individual respiratory complexes in the inner mitochondrial membrane suggested a dynamic array of structural and functional associations between different complexes, leading to the "plasticity model" that integrates the previously proposed "solid" and "fluid" models [16,17]. Recently, in support to the plasticity model of respiratory complexes organization, Lapuente-Brun et al. provided evidence for the interplay between SCs assembly and optimization of electron flux [18]. Accordingly, the SCs would define two functional CoQ sub-populations in the inner mitochondrial membrane, with a CoQ_{NADH} pool dedicated to reducing equivalents coming from NADH through CI-containing SCs, and a second separate CoQ_{FADH2} pool originating from $FADH_2$ through CII and other FAD-dependent enzymes to individual $CIII_2$ [18]. Consequently, the mitochondrial respiratory chain would be able to differently adjust the electron flow depending on whether SCs are present, or their assembly is prevented. The concept that CoQ could be compartmentalized within the mitochondrial membrane, and may have profound implications on cell metabolic adaptation, has been suggested earlier [19]. However, this issue is a matter of intense and controversial debate [4,5,15,20–22]. The recent structures of the mammal respirasome showed that the substrate-binding sites in CI and CIII are too far from each other, and separated by lipids without proteins that could facilitate channeling between them [4,23–26]. Furthermore, kinetic experiments on mitochondrial bovine particles demonstrated that CIII was completely reduced by both CI and CII related substrates [21], and that addition of an alternative oxidase competed with the NADH-linked oxidative phosphorylation (OXPHOS), providing evidence that quinone pool may not be compartmentalized [22].

Recently, we have characterized the effects of a novel pathogenic microdeletion in the *MT-CYB* gene that encompasses nucleotide positions 15,649–15,666 [27]. This microdeletion is located in the transmembrane helix six of cytochrome *b* subunit of CIII and causes the loss of six amino acids (Ile-Leu-Ala-Met-Ile-Pro; ΔI300-P305), leaving the remaining sequence in frame (Fig. 1, shown in red). As expected, the enzymatic activity of the mutated CIII was completely abolished in cybrid clones bearing the mutation in homoplasmy (i.e., 100% mutant mtDNA). Noticeably, immunoblotting analyses after SDS- or blue native (BN)-gel electrophoresis revealed that the content of $CIII_2$ was barely detectable in these cells [27,28]. However, the combined CI plus CIII enzymatic activity was not significantly different from control, whereas the combined CII plus CIII enzymatic activity was significantly reduced [27]. These findings prompted us to investigate in detail the possible change(s) in the supramolecular organization of SCs in the presence of this well-defined genetic alteration. Using the mutant mitochondria, we aimed to correlate the changes in the respiratory chain activity and OXPHOS with ensuing specific structural re-organizations of SCs. We report that, in addition to CIII, the assembly of CI and even more that of CIV was strongly impaired, even though a preferential structural interaction between CI and $CIII_2$ was preserved when CIII levels decreased. Moreover, we show that the stability of the individual complexes and their assembly into SCs are differently modulated in the mutant by inhibiting the electron transport through CI using rotenone, or by providing an antioxidant environment via incubation of cells with *N*-acetyl cysteine (NAC).

2. Materials and methods

2.1. Materials

ATP, ADP, malate, pyruvate, succinate, oligomycin, rotenone, P^1-P^5-di(adenosine-5′) pentaphosphate pentasodium salt, digitonin, dodecylmaltoside (DDM), Serva Blue G, aminocaproic acid, Bis-Tris, Ponceau S, glycerol, K-acetate, Hepes, phenylmethanesulfonyl fluoride (PMSF), *N*-acetyl cysteine (NAC); carbonyl cyanide 4-(trifluoromethoxy)phenylhydrazone (FCCP); Tris-Cl, NaCl, Na-deoxycholate, sodium dodecyl sulphate (SDS), 3-(4,5-dimethyl thiazol-2yl)-2,5-diphenyl tetrazolium bromide (MTT), EDTA, HEPES, sucrose, $MgCl_2$, KH_2PO_4, KCl, bovine serum albumin (BSA), erytrosine and the ATP monitoring kit were purchased from Sigma (Milan, Italy). ECL Western blotting kit was from Amersham Bioscience, Buckinghamshire, UK. Primary antibodies against CI (NDUFB6 and NDUFS3 subunits, cat. Ab110244 and cat. Ab. 110246, respectively), CIII (Core2 and UQCRC2 subunits, cat. Ab14745 and cat. Ab14745, respectively), CIV (Cox5A and Cox4 subunits, cat. Ab110262 and cat. Ab14744, respectively), CV (α subunit, cat Ab14748), VDAC (cat. 154856) were from Abcam, Cambridge, UK. Antibody against CII (SDHA subunit cat. 459200) was from Life Technologies, Milan, Italy. Antibody against Tim23 was from BD Biosciences, Milan, Italy. Antibody against peroxiredoxin 3 (PRX3) cat. LF-PA0030 was from ABfrontiers, South Korea. Anti-catalase cat. 505 and anti-glyceraldehyde 3-P dehydrogenase (GAPDH) cat. G8795 antibodies were from Sigma-Aldrich, Milan, Italy, and anti-actin cat.110246 antibody was from Protein Tech Manchester, UK. Horseradish peroxidase-conjugated secondary antibodies were from Jackson ImmunoResearch, West Grove, PA, USA.

2.2. Cell lines and culture conditions

The syngenic cybrid clones bearing the homoplasmic m.15,649–15,666 (I300-P305) microdeletion of *MT-CYB* (100% mutant, referred to as Δcytb 100%), the same deletion in heteroplasmy (80% mutant, Δcytb 80%) and the wild type (WT) mtDNA were all previously described [27]. In some experiments, two syngenic cybrid clones bearing the homoplasmic m.15579A > G (p.278Y > C) mutation of *MT-CYB* and its cognate WT mtDNA, were also used [29]. Cells were grown in Dulbecco's modified Eagle medium high glucose (DMEM) supplemented with 10% foetal calf serum (FBS), 2 mM L-glutamine, 100 U/mL penicillin, 100 μg/mL streptomycin (Life Technologies, Milan, Italy), in an incubator with a humidified atmosphere of 5% CO_2 at 37 °C. The growth medium of the Δcytb 100% mutant clones also contained 50 μg/mL uridine. Where indicated, confluent cells were incubated in DMEM in the presence of 1 μM FCCP for 24 h or 500 nM rotenone for 48 h [15] or 10 mM NAC for 72 h [13]. During NAC treatments, the medium was replaced after 48 h to avoid acidification.

2.3. One dimensional blue native-PAGE (1D BN-PAGE) and 2D BN/SDS-PAGE

Native complexes and SCs were analyzed in mitochondria-enriched fractions obtained from cell pellets (approximately 10×10^6 cells) using digitonin (final concentration 50 μg/mL) as previously described [29,30]. For native complexes, mitochondrial fractions were suspended in mitochondrial buffer containing 750 mM aminocaproic acid, 50 mM

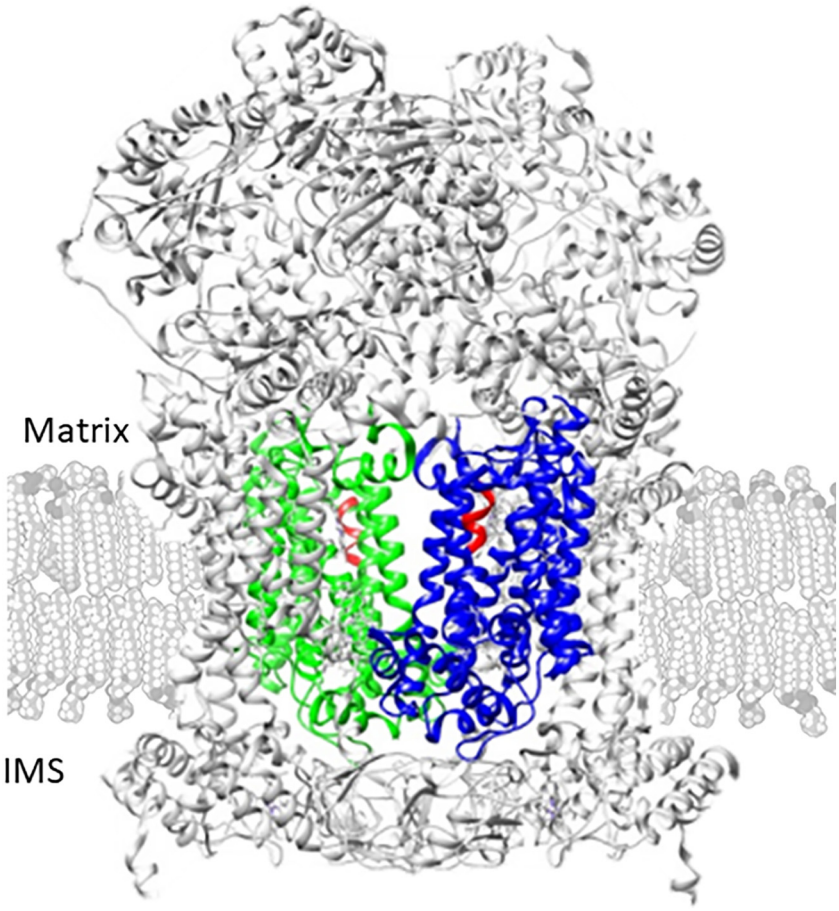

Fig. 1. Location of cytochrome *b* microdeletion in human $CIII_2$ structure.
Depiction of the location of cytochrome *b* microdeletion using the structure of human $CIII_2$ (PDB ID: 5XTE). The six amino acid long deletion (ΔI300-P305) is located on the transmembrane helix six of cytochrome *b* (blue and green subunits in each monomer) subunits, and shown in red. (For interpretation of the references to color in this figure, the reader is referred to the web version of this article.)

Bis-Tris, pH 7.0, and solubilized by adding dodecylmaltoside (DDM) at a DDM/protein ratio of 2.5 (g/g). The suspension was incubated on ice for 10 min and then centrifuged at 13000*g* for 15 min [29,30]. The supernatants were used for analysis of isolated complexes by Blue Native (BN)- or Clear Native (CN)-PAGE. About 80 μg of protein were loaded onto a 4–12% gradient gel after addition of sample buffer (for BN-PAGE: 5% Serva Blue G in 750 mM aminocaproic acid, 50 mM Bis-Tris, 0.5 mM EDTA, pH 7; for CN-PAGE: 0,1% Ponceau S in 50% glycerol). Samples were loaded in duplicate onto CN- and BN-PAGE as described in Ghelli et al. and Wittig et al. [29,30]. After electrophoresis, the CN-PAGE gels were utilized for determination of CI in-gel-activity (CI-IGA) and the BN-PAGE gels were used for western blot analyses. The CI-IGA was assessed by the NADH/MTT reductase activity, incubating the gels with 5 mM Tris-Cl (pH 7.4), 0.15 mM NADH, and 2.5 mg/mL MTT at room temperature. The reaction was stopped with 50% methanol and 10% acetic acid, and the gel was analyzed with a Fluo-2 MAX multi-imager system (Bio-Rad) [31].

For the analyses of SCs, mitochondria-enriched fractions obtained by digitonin treatment were suspended in PBS and protein content was determined. After centrifugation, the pellet was suspended in 150 mM K-acetate, 30 mM HEPES, pH 7.4, 10% glycerol, 1 mM PMSF, 10 mg/mL digitonin (digitonin/protein ratio of 2 g/g) and incubated on ice for 30 min [29,30]. Samples were centrifuged for 2 min at 600*g*, and supernatants were used for BN-PAGE and BN/SDS-PAGE. About 20 μg of proteins were loaded onto a 3–12% gradient gel (BN-PAGE) after addition of 5% Serva Blue G in 750 mM aminocaproic acid [29,30]. After electrophoresis, gels were processed for CI-IGA [31] and western blot analyses or second dimension SDS-PAGE (2D BN/SDS-PAGE). Strips from the first dimension 3–12% gradient gel were excised and used for 2D BN/SDS-PAGE. Each strip was treated with the denaturing buffer containing 1% SDS and 0.1% β-mercaptoethanol for 90 min and separated using a 10% SDS-PAGE as described in Ghelli et al. and Wittig et al. [29,30]. After electrophoresis, gels were used for western blot analyses.

2.4. SDS-PAGE and western blot analyses

Mitochondria-enriched fractions were solubilized in RIPA buffer (50 mM Tris-HCl pH 7.4, 150 mM NaCl, 1% NP-40, 1% Na-deoxycholate, 1% SDS, 5 mM EDTA), and their protein content was measured. Proteins (40 μg) were separated using a 12% SDS-PAGE and transferred onto a nitrocellulose membrane (Bio-Rad, Hertfordshire, UK) for western blotting analyses. The nitrocellulose membranes were incubated overnight at 4 °C with antibodies for CI (NDUFB6 or NDUFS3 subunits 1:1000), CII (SDHA subunit 1:10000), CIV (Cox5A or Cox4 subunit 1:1000), CIII (Core2 subunit 1:1000; UQCRC2 1:1000), VDAC (1:10000), Tim23 (1:1000), PRX3 (1:2000), catalase (1:4000), GAPDH (1:20000) and actin (1:5000). Primary antibodies bound to their corresponding antigens were visualized using horseradish peroxidase-conjugated secondary antibodies (1:2000). The chemiluminescence signals were revealed by an ECL western blotting kit and measured with Gel Logic 1500 Imaging System (Kodak, Rochester, NY, USA).

2.5. In vivo labelling of mitochondrial translation products

The in vivo labelling of mitochondrial translation products was performed essentially as described in Sasarman and Shoubridge [32]. Two days prior to the experiment, $2{,}5 \times 10^5$ cells per well were seeded in 12-well plates. Just before labelling, the growth medium was removed and cells were rinsed twice with fresh DMEM lacking methionine and serum. Labelling medium (0.75 mL of methionine-free DMEM supplemented with 10% FBS) was added, and cells were incubated for

15 min at 37 °C. Then 200 μg/mL emetine and 100 μg/mL cycloheximide were added, and incubation was extended for another 10 min. Labelling was performed by incubating cells for 45 min at 37 °C after the addition to each well of 300 μCi/mL of EasyTag™ L-[^{35}S]-methionine (PerkinElmer), followed by 10 min chase in 2 mL fresh complete DMEM supplemented with 10% FBS. Cells were first washed three times, resuspended in phosphate buffered saline (PBS) using 0.5% trypsin, and washed two more times with PBS. Each pellet was lysed in Laemmli buffer, and proteins were loaded on 15%–20% SDS-PAGE. Dried gels were analyzed by phosphor imaging using Typhoon FLA 9500 and ImageQuant TL Software. The intensity of the bands obtained with Coomassie blue-staining of proteins was used as loading control. For quantification of the relative protein synthesis rate, the value of intensity of each radioactive band of 80% and 100% mutants, was normalized for Coomassie blue-staining (load control), and indicated as mean ± SD. Values are expressed as a ratio on WT cells.

2.6. Oxygen consumption rate

The rate of oxygen consumption was measured in digitonin-permeabilized cells essentially as described in [33]. Briefly, about 5×10^6 cells were harvested and suspended at a concentration of 10×10^6/mL in a buffer containing 20 mM HEPES pH 7.2, 250 mM sucrose, 10 mM $MgCl_2$. Cells were permeabilized with 50 μg/mL digitonin, incubated for 1 min at room temperature, then diluted with 2.5 volume of buffer, and permeabilization was monitored by erythrosine b staining. Cells were centrifuged at 10000*g* for 1 min and suspended in the same buffer at the concentration of 10×10^6/mL. The permeabilization protocol was repeated until 90–100% of cells were positive to erythrosine b staining. Permeabilized cells were then centrifuged at 10000*g* for 1 min and suspended in 1.9 mL of the same buffer supplemented with 2 mM KH_2PO_4 pH 7.2 and 1 mM ADP (respiration buffer), and the suspension was introduced into the Clark electrode chamber at 37 °C. After about 1–2 min of base line recording, substrates were added as follows: 5 mM malate plus 5 mM pyruvate (CI substrates); 5 mM succinate (CII substrate) plus 2 μg/mL rotenone; 5 mM malate, 5 mM pyruvate plus 5 mM succinate (CI + CII substrates). The rates of oxygen consumption were normalized to protein content considering that citrate synthase activity, an indicator of mitochondrial mass, was similar in all cell lines.

2.7. Mitochondrial ATP synthesis

The rate of mitochondrial ATP synthesis was measured in digitonin-permeabilized cells by using the luciferin/luciferase assay, as previously described [34]. Briefly, after trypsinization, cells (10×10^6/mL) were suspended in a buffer containing 150 mM KCl, 25 mM Tris-HCl, 2 mM EDTA, 0.1% bovine serum albumin, 10 mM KH_2PO_4, 0.1 mM $MgCl_2$, pH 7.4, kept at room temperature for 15 min, then incubated with 50 μg/mL digitonin until 90–100% of cells were positive to erythrosine b staining. Aliquots of 3×10^5 permeabilized cells were incubated in the same buffer in presence of the adenylate kinase inhibitor P^1,P^5-di(adenosine-5′) pentaphosphate (0.1 mM). Substrate concentrations were as follows: 1 mM malate plus 1 mM pyruvate (CI substrates); 5 mM succinate (CII substrates) plus 2 μg/mL rotenone; 1 mM malate, 1 mM pyruvate and 5 mM succinate (CI + CII substrates). After addition of 0.1 mM ADP, chemiluminescence was determined as a function of time with a luminometer. The chemiluminescence signal was calibrated using an internal ATP standard after addition of 10 μM oligomycin. The rates of ATP synthesis were normalized to protein content considering that citrate synthase activity was similar in all cell lines.

2.8. Dicarboxylic acids determination by LC-MS/MS

The measurements were carried out essentially as previously described [28,35]. Approximately 10^7 cells were washed with ice-cold PBS, centrifuged and suspended in 1 mL PBS. An aliquot was kept for protein determination. The subsequent procedures were carried out at 4 °C. After centrifugation at 600*g*, the supernatant was removed and 1 mL cold methanol/acetonitrile (1:1) was added. The pellet was carefully mixed, and then centrifuged at 13000*g* for 5 min. The supernatant was evaporated under a nitrogen stream, and the dry extracts were used for LC-MS/MS analysis, as previously described [35].

2.9. Statistics analysis

Data are presented as means ± standard deviation (SD). Statistical analysis was performed using the One sample or Two samples *t*-test with $p < 0.05$ as the level of significance. Number of biological replicates in independent experiments is detailed in each figure legend.

3. Results

3.1. Mutation-load related strong reduction of CI, CIII and CIV

In order to shed light on effects of the *MT-CYB* microdeletion on the structural organization of the OXPHOS system, we first analyzed the assembly status of the OXPHOS complexes in the syngenic clones bearing the microdeletion in homoplasmic (100% of mutated mtDNA, Δcytb 100%) and heteroplasmic (80% of mutated mtDNA, Δcytb 80%) states. BN-PAGE of samples of the three cybrid clones solubilized with DDM was utilized (Fig. 2A). The CI-In-Gel Activity (CI-IGA) was barely detectable in Δcytb 100% clone compared to WT and Δcytb 80% clones. Western blot analysis confirmed that the CI band intensity (i.e., NDUFB6-CI panel) significantly decreased with increasing mutation load, being very faint in the homoplasmic mutant clone (Fig. 2A; quantification in panel C). Similar results were obtained with the band intensity of the individual $CIII_2$ (i.e., UQCRC2-CIII), being rather weak in Δcytb 100% cells. Noticeably, the signal of $CIII_2$ + CIV SC was barely visible in Δcytb 80% and virtually absent in Δcytb 100% clones. Accordingly, the CIV (i.e., COX5A-CIV) also exhibited a similar pattern, being almost undetectable in Δcytb 100% cells (Fig. 2A and C). Conversely, the levels of assembled CII and CV were only weakly affected (Fig. 2A, i.e., SDHA-CII and subunit α-CV).

In parallel, we examined the supramolecular organization of the OXPHOS complexes in the same samples of the three cybrid clones, after solubilization with the mild detergent digitonin (2 g/g protein) instead of DDM (Fig. 2B). In the CI-IGA panel, the SCs containing active CI were detected in all clones, although remarkably less in the Δcytb 100%. This behavior was mirrored by western blot analysis, as reported in Fig. 2B and quantified in panel D. Intriguingly, the Δcytb 100% and especially the Δcytb 80% mutant clone also exhibited an unusually high molecular weight SC (called super-SC, SSC), which seemed to be barely detectable, if at all, in the WT cells. Although the basis of the occurrence of SSC is unclear, its presence in cells carrying the *MT-CYB* microdeletion either alone (Δcytb 100%), or in the presence of wild-type cytochrome *b* (Δcytb 80%), suggested that the mutant form of $CIII_2$ interfered with the formation of SCs, leading to SSC accumulation. Interestingly, in the mutants, the $CIII_2$ was present in the SCs only, being more abundant in the Δcytb 80% and scarce in the Δcytb 100% clone (Fig. 2B and D), primarily preserving its interaction with CI. In agreement with the results of Fig. 2A, CIV was almost absent in the Δcytb 100% cells, whereas the amount of individual CIV as well as that associated to the SSC slightly increased in the Δcytb 80% cells (Fig. 2B and D). Finally, CV was present in two bands, corresponding to the dimer (CV_2) and the monomer. The amount of CV_2 slightly decreased in the mutants, whereas that of the CV monomer somewhat increased. The levels of CV therefore, do not appear to be significantly influenced by the *MTCYB* microdeletion, in agreement with the in vitro translation results (see below).

These findings were also confirmed by the 2D BN/SDS-PAGE (BN-PAGE followed by SDS-PAGE) analysis, and detection of representative

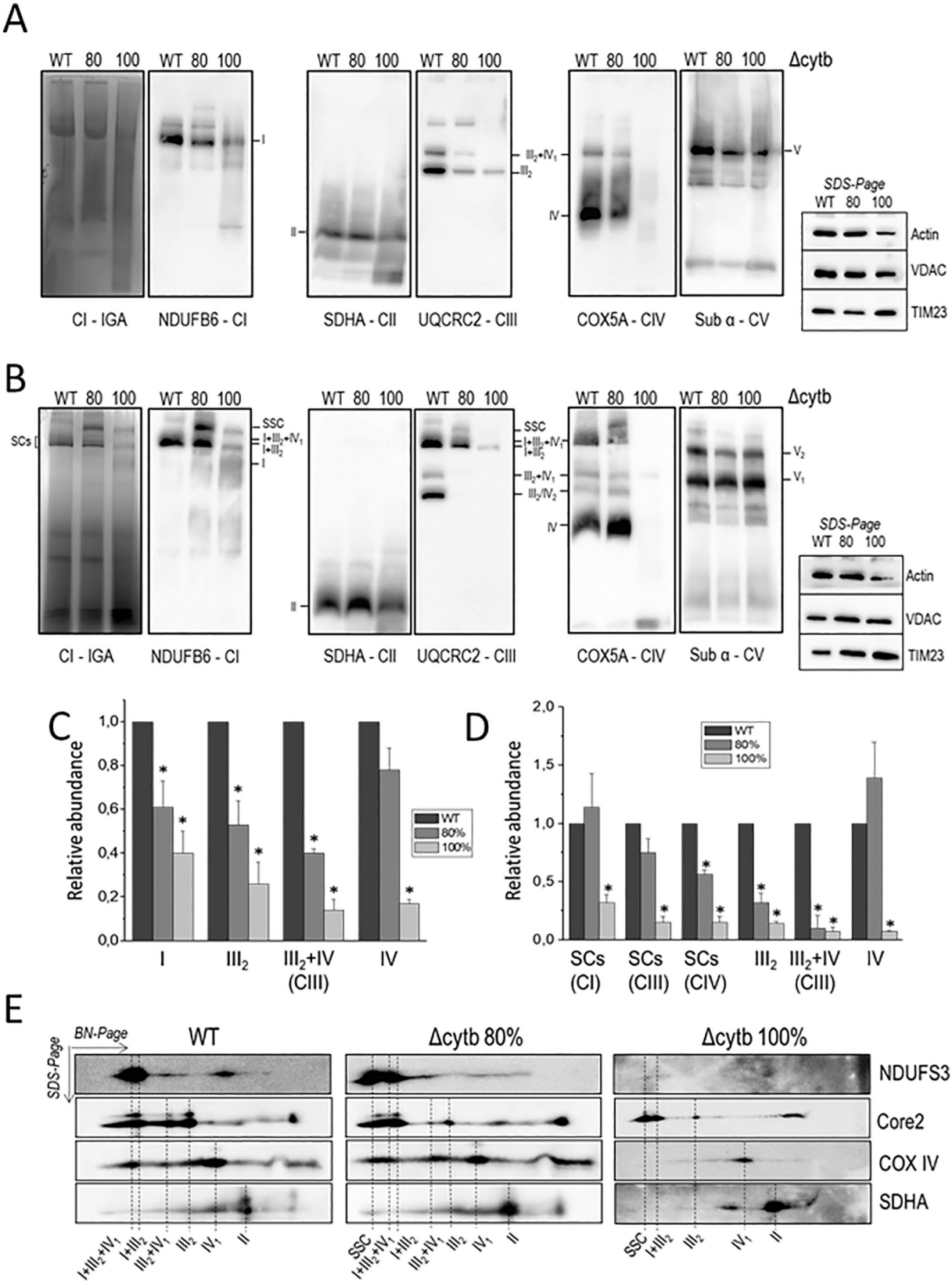

(caption on next page)

subunits of respiratory complexes by immunoblotting (Fig. 2E). The SCs containing CI, CIII and CIV were indeed present in WT and Δcytb 80%, but not in Δcytb 100% clone where only the CI + $CIII_2$ SC was clearly detectable. In addition, in agreement with the panel 2B results, the SSC was especially present in the Δcytb 80% mutant (Fig. 2E). Moreover, the spots corresponding to $CIII_2$ and to the $CIII_2$ + CIV SC were reduced in the Δcytb 80%, and almost absent in the Δcytb 100% clone. The detection of a spot attributed to CIV in the 2D BN/SDS-PAGE blots, and

Fig. 2. Expression level and assembly of OXPHOS complexes and SCs.
A) Aliquots of DDM-solubilized mitoplasts isolated from WT, Δcytb 80% and Δcytb 100% cybrids, were separated by BN-PAGE. For each experiment, three different gels were loaded with the same samples. One gel was used for the CI in-gel-activity (CI-IGA), as described in Materials and Methods. The other gels were transferred into nitrocellulose membrane for western blot analysis, using antibodies against the indicated subunits of OXPHOS complexes. Blots are representative of at least three biological replicates in independent experiments; images of membranes were acquired after ~60s of exposition. Where indicated, SDS-PAGE and western blot analysis of the same samples was carried out using the indicated antibodies.
B) Aliquots of digitonin-solubilized (2 g/g protein) mitoplasts isolated from WT, Δcytb 80% and Δcytb 100% cybrids, were separated by BN-PAGE, and treated exactly as described in A). Blots are representative of at least three independent experiments; images of membranes were acquired after ~60s exposition. The signals of different complexes in DDM- (C) and of complexes/SCs in digitonin-solubilized (D) mitochondria were quantified by densitometry, after normalization by CII, and indicated as mean ± SD. Values are expressed as a ratio on WT cells. Statistical analysis was performed using the One sample *t*-test; * indicates $p < 0.05$ as the level of significance.
E) 2D BN/SDS-PAGE analysis of respiratory SCs was carried out in aliquots of digitonin-solubilized mitochondria separated by BN-PAGE. Strips excised from the gels were resolved by second dimension SDS-PAGE. Spots were detected with antibodies against the indicated subunits of CI, CII, CIII and CIV. Blots are representative of three biological replicates in independent experiments; images of membranes were acquired after ~60s of exposition for WT and Δcytb 80% and 120 s for Δcytb100% cybrids.

the lack of CIV seen in Fig. 2B, is ascribed to the fact that these datasets were acquired at different exposure times (i.e., longer in the 2D experiments), revealing the trace amounts of CIV not detected in Fig. 2B.

Taken together overall results indicated that in cells bearing the *MT-CYB* microdeletion, SCs undergo re-organization, partly preserving CI and CIII interactions while forming a very high molecular weight aggregate (SSC) at the expense of the almost complete disassembly of other CIII and CI involving complexes. Furthermore, the quasi-absence of CIV suggested that the *MT-CYB* microdeletion strongly affected CIV levels and the interactions between $CIII_2$ and CIV more severely than those between CI and $CIII_2$ during SC formation. This observation is in agreement with the presence of only trace amount of CI + $CIII_2$ and $CIII_2$ + CIV SCs, and lack of detection of the CI + $CIII_2$ + CIV respirasome, in the Δcytb 100% clones (Fig. 2B).

To evaluate the mechanism involved in the dramatic perturbation of respiratory complexes assembly and organization, we performed in vivo labelling of mitochondrial polypeptides by incubating cells with ^{35}S-methionine in the presence of cycloheximide and emetine [32]. As shown in Fig. 3A, the overall patterns of the translation products from mutation-carrying cybrids were qualitatively identical to WT in terms of their electrophoretic mobility. Quantification of bands intensity revealed that in the Δcytb 80% cells, the rate of synthesis of the CI and CIII mtDNA-encoded subunits was increased, in particular that of cytochrome *b*, in line with a possible compensatory effect (Fig. 3B). Conversely, in the Δcytb 100% cells, a significant reduction in the synthesis rate was observed for CI, CIV subunits and cytochrome *b*, whereas the synthesis of the subunits of CV was not affected (Fig. 3B). These findings suggest that the presence of the homoplasmic *MT-CYB* microdeletion significantly affects the mitochondrial biosynthesis and consequently contributes to the reduction of their amounts (Fig. 2).

3.2. Rates of electron flux through CI and CII

Considering the ongoing debate on whether the ubiquinone pool is partitioned between distinct respiratory pathways, we thought that our *MT-CYB* microdeletion clones with their well-defined genetic alteration leading to defective CIII assembly and SCs re-organization, might provide additional insights. Namely, the possible co-existence of two distinct routes, corresponding to one from NADH through the respirasome and one from $FADH_2$ to free CIII and CIV, were examined [18]. Using digitonin-permeabilized cells, we measured the rate of oxygen consumption and ATP synthesis driven by NADH-linked (i.e., pyruvate/malate) or the $FADH_2$-linked (i.e., succinate) substrates or both, in the presence of saturating concentration of ADP (state 3). Fig. 4A shows that the rates of oxygen consumption driven by CI (i.e., pyruvate + malate) or CII (i.e., succinate) were similar in WT and Δcytb 80%. In the presence of both pyruvate/malate and succinate, the rates in WT cells increased, but were not additive; conversely, no increase was seen in Δcytb 80% clone (Fig. 4A). Similarly, the rates of CI (i.e., pyruvate + malate) or CII (i.e., succinate) driven ATP synthesis were comparable between the WT and Δcytb 80% clones. Moreover, no additivity in the ATP synthesis was observed by simultaneous addition of CI and CII substrates (i.e., pyruvate + malate + succinate) in both WT and Δcytb 80% clones (Fig. 4B), similar to oxygen consumption rates (Fig. 4A). In the Δcytb 100% clone, no CI- or CII-driven oxygen consumption rate was detected, likely due to the very low amount of CIII and CIV that hampers the electron transport through the respiratory chain (Fig. 4A). However, we note that in the Δcytb 100% clone, although the CI-driven ATP synthesis was extremely reduced as compared with WT, it was still detectable using a highly sensitive bioluminescence based assay. Probably, the low CI, CIII and CIV residual activities were able to produce enough proton gradient for ATP synthesis, as previously reported [27]. Conversely, the CII-driven ATP synthesis was undetectable (Fig. 4B). Note that when the CI and CII substrates were simultaneously added, ATP synthesis was completely abolished, suggesting that ATP synthesis driven by malate + pyruvate is inhibited by the presence of succinate, possibly leading to more $CoQH_2$ generation via CII (Fig. 4B).

Taken together, these results indicate that, within the error bars, there is no difference in oxygen consumption and ATP synthesis rates between the WT and 80% mutant and no additivity when both substrates are added, suggesting that the NADH and $FADH_2$ oxidation routes compete for the same Q-pool, which is not compartmentalized.

In order to shed further light to the electron flux through CI and CII, we used another cybrid cell line bearing the homoplasmic p.278Y > C missense mutation in the *MT-CYB* gene [29]. Earlier we had shown that this mutation strongly reduces CIII enzymatic activity, without changing substantially the CI or CIII assembly. These cells exhibited decreased amounts of $CIII_2$ and $CIII_2$ + CIV SC, but preserved the CI + $CIII_2$ + CIVn SCs [29]. As reported in Fig. 4C and D, cells carrying *MT-CYB* p.278Y > C missense mutation showed significant but similar decreases of oxygen consumption and ATP synthesis driven by CI and CII substrates as compared with WT cells. This finding indicated that the CIII that was preferentially included into the CI + III_2 + IVn SCs remained active to oxidize reduced CoQ_2 generated by both CI and CII activities [29]. We note that the rates of oxygen consumption and ATP synthesis increased in WT, but not in mutant cell lines upon simultaneous addition of the CI and CII substrates (i.e., pyruvate + malate + succinate). This result is consistent with the occurrence of a mutual inhibition between NADH:O_2 (CI-dependent) and succinate:O_2 (CII-dependent) pathways when CIII activity becomes limiting, which might indicate the presence of common and not partitioned Q pool [21,22], as above.

3.3. Reverse electron transfer is not involved in SCs stabilization

Recently, Guaras et al. proposed that respiratory complex defects causing increased $CoQH_2$/CoQ ratio induce CI degradation, triggered by superoxide overproduction generated by RET. In particular, it has been shown that the CI inhibitor rotenone stabilizes CI assembly possibly through reducing RET [15]. We reasoned that Δcytb 100% cybrids

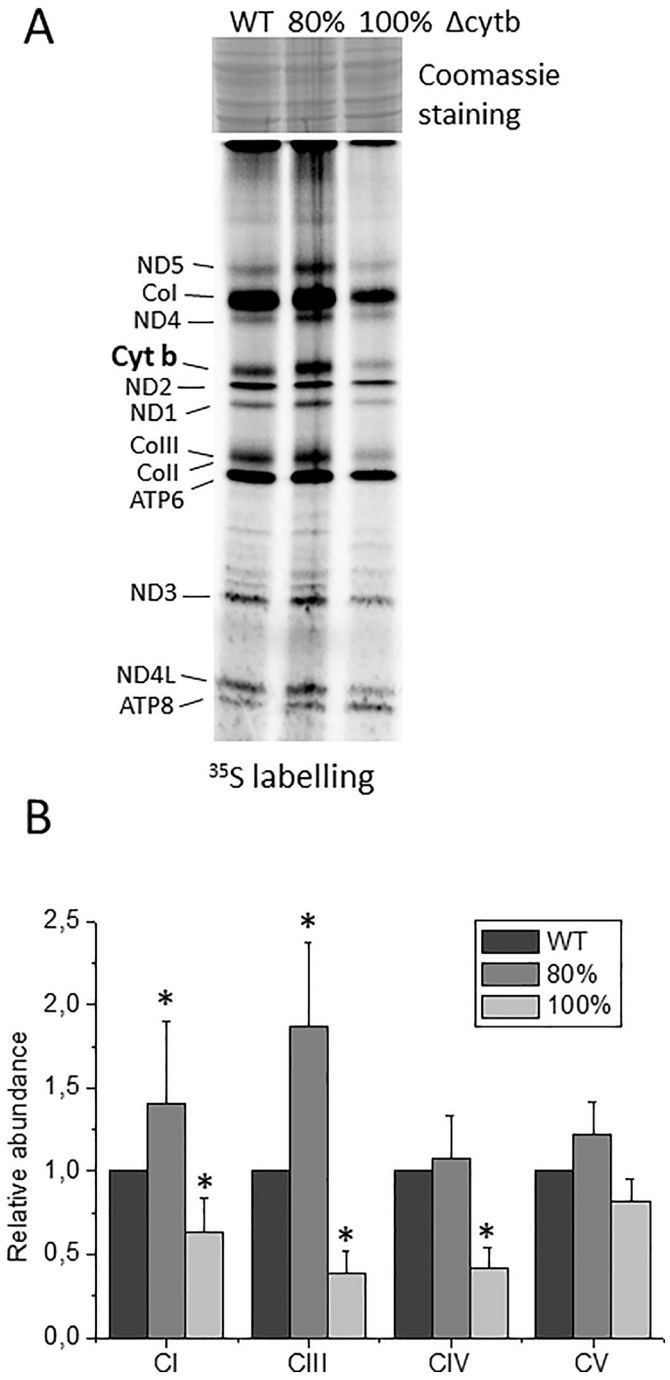

Fig. 3. De novo synthesis of mtDNA-encoded polypeptides.
A) Pattern of the radiolabelled mitochondrial translation products on gradient polyacrylamide-SDS gel from WT, Δcytb 80% and Δcytb 100% cybrids. In the upper part, the corresponding Coomassie blue-stained gel is shown as a control for loading. B) Quantitative analysis of the rates of synthesis of the mt-DNA-encoded subunits in Δcytb 80% and Δcytb 100% cybrids, relative to WT, determined as described in the Materials and Methods section. Data are means ± SD of five biological replicates in independent experiments. Statistical analysis was performed using the One sample *t*-test; * indicates $p < 0.05$ as the level of significance.

might represent a good cell model to further probe this finding, as a severe defect of CIII enzymatic activity is thought to yield an increased $CoQH_2/CoQ$ ratio, which in turn could enhance oxidative stress by RET. Indeed, we have reported that such cells do not present any perturbation in reduced (GSH) and oxidized (GSSG) glutathione contents, and in the GSSG/GSH ratio. However, they exhibit increased levels of cytosolic (catalase) and mitochondrial (peroxiredoxin 3, PRX3) antioxidant enzymes compared to control cells, suggesting that they undergo oxidative unbalance [28]. More recently, the occurrence of oxidative stress in these cells has been directly demonstrated through the use of novel time-resolved chronoamperometric measurements, revealing enhanced H_2O_2 production in digitonin-permeabilized Δcytb 100% cybrids compared with controls [28,36].

Given that RET is inhibited by uncouplers such as FCCP, or by CI inhibitors like rotenone, we tested the effect of these compounds on the levels of these antioxidant enzymes in Δcytb 100% cell line. Pre-incubation with 1 μM FCCP (24 h) or 500 nM rotenone (48 h) had no significant effect on catalase and PRX3 expression (Fig. 5A–C). These results suggested that in our cell model, oxidative stress is not RET dependent, as neither FCCP nor rotenone was effective on reducing the expression of either cytosolic or mitochondrial antioxidant enzymes. We then tested whether the assembly of CI could be modified by the presence of FCCP, by measuring the CI-IGA after clear native (CN)-PAGE of DDM-solubilized mitochondria, as shown in Fig. 5D. The weak CI-IGA of Δcytb 100% cybrids was further reduced by incubation with FCCP, and no significant effect was apparent in WT and Δcytb 80% cells. Moreover, FCCP had no effect on the CI-containing SCs isolated in digitonin-solubilized mitochondria, as evidenced by CI-IGA (Fig. 5E).

3.4. Fine-tuning of the organization of respiratory SCs and increased energetic efficiency in the presence of NAC

Next, we tested the effect of rotenone on the DDM-isolated OXPHOS complexes of the Δcytb 100% cybrids, showing that this inhibitor significantly increased the amount of CI and, much less of $CIII_2$, whereas that of CIV was almost undetectable (Fig. 6A; quantification in panel C). We previously reported that prolonged incubation with NAC significantly reduces PRX3 expression levels in Δcytb 100% cybrids [28]. Thus, we also measured the effect of 72 h incubation of Δcytb 100% cybrids with 10 mM NAC, which evidenced a weak increase in the band intensity of isolated CI, $CIII_2$, whereas the levels of CIV were similar to control cells (Fig. 6A and C). Then, we analyzed whether these two treatments could also influence the organization of the SCs. Fig. 6B,D shows that the SCs content, evaluated by CI-IGA and CIII (i.e., UQCRC2-CIII), was not significantly enhanced by the two treatments, whereas NAC significantly increased the SCs CIV content, suggesting the occurrence of partial re-assembly of the respirasome. Moreover, both compounds increased the amount of $CIII_2$ (approximately 1.5- and 2-fold increase with rotenone and NAC, respectively, Fig. 6B, D). Conversely, incubation with rotenone decreased while NAC increased the CIV_2 content (Fig. 6B, D). We note that the presence of CIV signals in the Δcytb 100% cybrids could be detected (Fig. 6) as the blots signals were acquired at longer times in this case than in Fig. 2 (60 and 120 s, respectively). We add that both treatments induced a similar increase in CI and $CIII_2$ also in WT and Δcytb 80% cybrids (results not shown), suggesting that this is a general effect, although further studies are required to evaluate the mechanism involved.

Given that in Δcytb 100% cells the CI-driven ATP synthesis was not completely abolished but reduced to about 10% of that seen with WT cells (Fig. 4B), we decided to investigate whether NAC could also ameliorate the energetic efficiency of these cells. After treatment with NAC, the ATP synthesis rate driven by pyruvate + malate was increased > 2-fold compared with untreated cell (Fig. 6E), likely as a consequence of partial re-assembly of the respirasome as well as of $CIII_2$ and CIV_2. Previously, we reported a significant accumulation of succinate (8-fold increase over WT cells) in the Δcytb 100% cell line, likely due to the blockage of electron flux at the CIII level [28]. Fig. 6F reports the levels of succinate together with fumarate and malate after 72 h incubation with NAC, showing a markedly decrease in the succinate levels, strongly supporting the notion that the partial re-assembly of the respirasome can improve re-oxidation of $CoQH_2$ leading to succinate

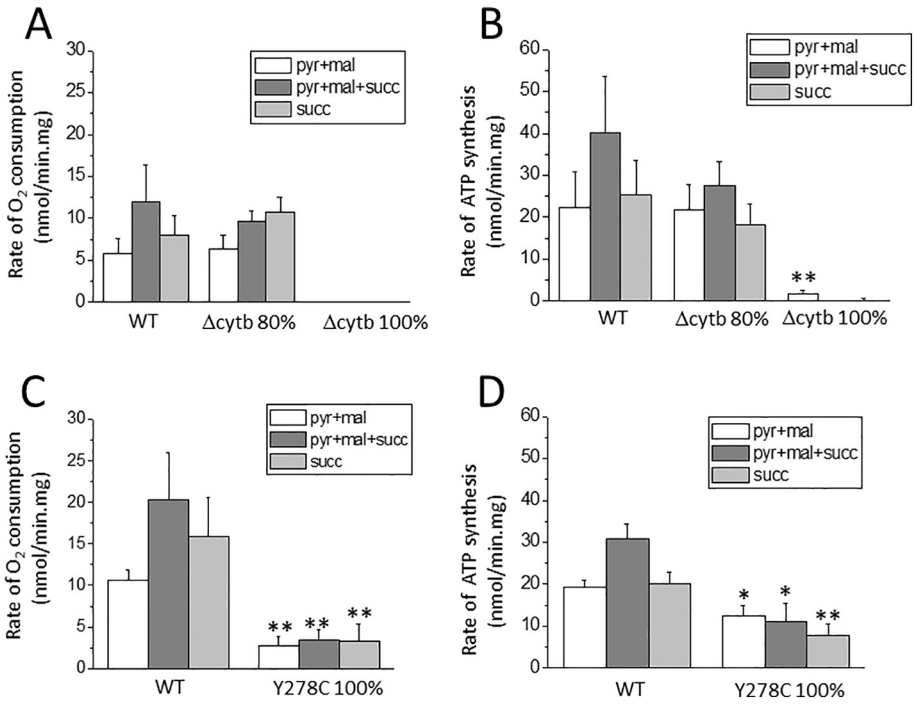

Fig. 4. Oxygen consumption and ATP synthesis rates.

A, C) Oxygen consumption rates driven by malate + pyruvate (CI substrates) or succinate (CII substrate) or both were measured in digitonin-permeabilized cybrids (see Materials and Methods) by using a Clark electrode at 37 °C. B, D) Rates of ATP synthesis driven by malate + pyruvate (CI substrates) or succinate (CII substrate) or both were determined in digitonin-permeabilized cells, as detailed in Material and Methods. Data are means ± SD of at least six independent experiments. Statistical analysis was performed using the Two samples *t*-test. Asterisks denote values significantly different from WT cells $^{*}p < 0.05$ and $^{**}p < 0.01$.

A, B) Cybrids bearing WT mtDNA and isogenic Δcytb 80% or Δcytb 100% cybrids were used; C, D) cybrids bearing WT mtDNA and the isogenic clone with the homoplasmic *MT-CYB* p.Y278C missense mutation were used.

consumption.

4. Discussion

In this study, we investigated in detail the re-organization of SCs when CIII assembly is hampered by a *MT-CYB* gene microdeletion causing the loss of 6-amino acids in the structural subunit cytochrome *b* [27], and the functional consequences of this re-organization on the respiratory and OXPHOS functions. First, we confirm that, although most of CI, CIII and CIV are not present, a preferential structural interaction between CI and $CIII_2$ is seen (see the model proposed in Fig. 7A), as reported earlier [18]. This allows a residual CI + CIII combined redox activity, and an associated low but detectable ATP synthesis driven by CI substrates only (Carossa et al. [27] and this work). This result supports our previous hypothesis that the assembly of $CIII_2$ into the CI + $CIII_2$ SC could mitigate the detrimental effect of *MT-CYB* mutations [29,37]. This observation nicely corroborates the assumption that the evolutionarily conserved CI + $CIII_2$ core complexes might play an important role in respiratory electron transfer and respiratory complexes stability [4,5,23,38]. We also noticed the occurrence of a very large molecular weight SC (SSC) containing CI, CIII and CIV that is clearly visible in the Δcytb 80% mutant cells. The composition, relative stoichiometry and activity of the respiratory complexes present in the SSC need to be defined in future studies, which however, are beyond the scope of the current work.

Another unexpected observation that emerged during this work is that in cells with the homoplasmic microdeletion, differently from those harboring other *MT-CYB* mutations [9,39], the CIV level decreased even more markedly than the CIII itself. Indeed, a strong reduction of both CI and CIV assembly was reported in mouse fibroblasts lacking Rieske iron-sulfur protein, which was associated with the occurrence of an oxidative stress [13]. Note that an oxidative unbalance was demonstrated also in Δcytb 100% cybrids [28,36], which might thus contribute to increased CI and CIV instability. In addition, the experiments of mitochondrial de novo protein synthesis indicate that the *MT-CYB* microdeletion significantly affects the rate of CI and CIV subunits biosynthesis, and consequently, the expression levels of these complexes. Indeed, alterations in mitochondrial transcription efficiency induced by mtDNA point mutations or microdeletions have already been reported [40]. However, the finding that the mtDNA encoded CV subunits biosynthesis is not affected by the *MT-CYB* deletion is not in concordance with this hypothesis, suggesting that further studies are needed to define the underlying mechanism(s). Therefore, we can only speculate that the combined effects of decreased expression levels of mtDNA encoded proteins, supplemented with the increased ROS production could rationalize the observed pronounced reduction of the CI and CIV levels. Finally, we cannot rule out that the mitochondrial perturbations associated with the *MT-CYB* microdeletion might induce changes in the levels of SCs assembly factors, such as HIGD2A or COX7A2L/SCAF1, loosening the interactions of CIV within the respirasome [39,41]. This topic clearly deserves further studies.

The second finding of this work provides evidence that quinone pool may not be compartmentalized, in contrast with previous reports by Lapuente-Brun et al. [18], who showed that a 70% reduction of CIII still maintained the CI + $CIII_2$ + CIV_n SC assembly and CI + CIII activity, but strongly reduced CII + CIII activity. In disagreement with those results, we show that in cells with Δcytb 80% mutation load, despite the preferential association of CI and CIII and the quasi-absence of $CIII_2$ + CIV SC, the electron flow and ATP synthesis through CI and CII were similar. Furthermore, in the presence of both CI and CII substrates, the rates of oxygen consumption and ATP synthesis in WT and mutant cells were lower than the sum of the rates measured when the NADH:O_2 and succinate:O_2 pathways operate independently. In our opinion, the functional evidence here reported is consistent with the presence of a free Q-pool, although these results do not provide any definitive evidence, leaving this issue unsolved for the time being [4,5].

The third important finding of this study concerns the effect of either rotenone or NAC, showing that although both stabilize the assembly of single CI and $CIII_2$, they probably affect CIV differently, and subsequently, they act on the SCs organization via different mechanisms. In fact, only NAC, and not rotenone, was able to promote partial re-assembly of the respirasome, significantly ameliorating the energetic function, whereas rotenone was ineffective (see Fig. 7B and C). Thus, we suggest that rather than inhibiting RET, rotenone might recruit and stabilize the inactive Q and P_p modules of CI in the early stages of its assembly by interacting with the ND1, NDUFS2, NDUFS7 and NDUFS8 subunits predicted to form the quinone binding pocket [42–46]. In support of this hypothesis, recent photoaffinity labelling studies

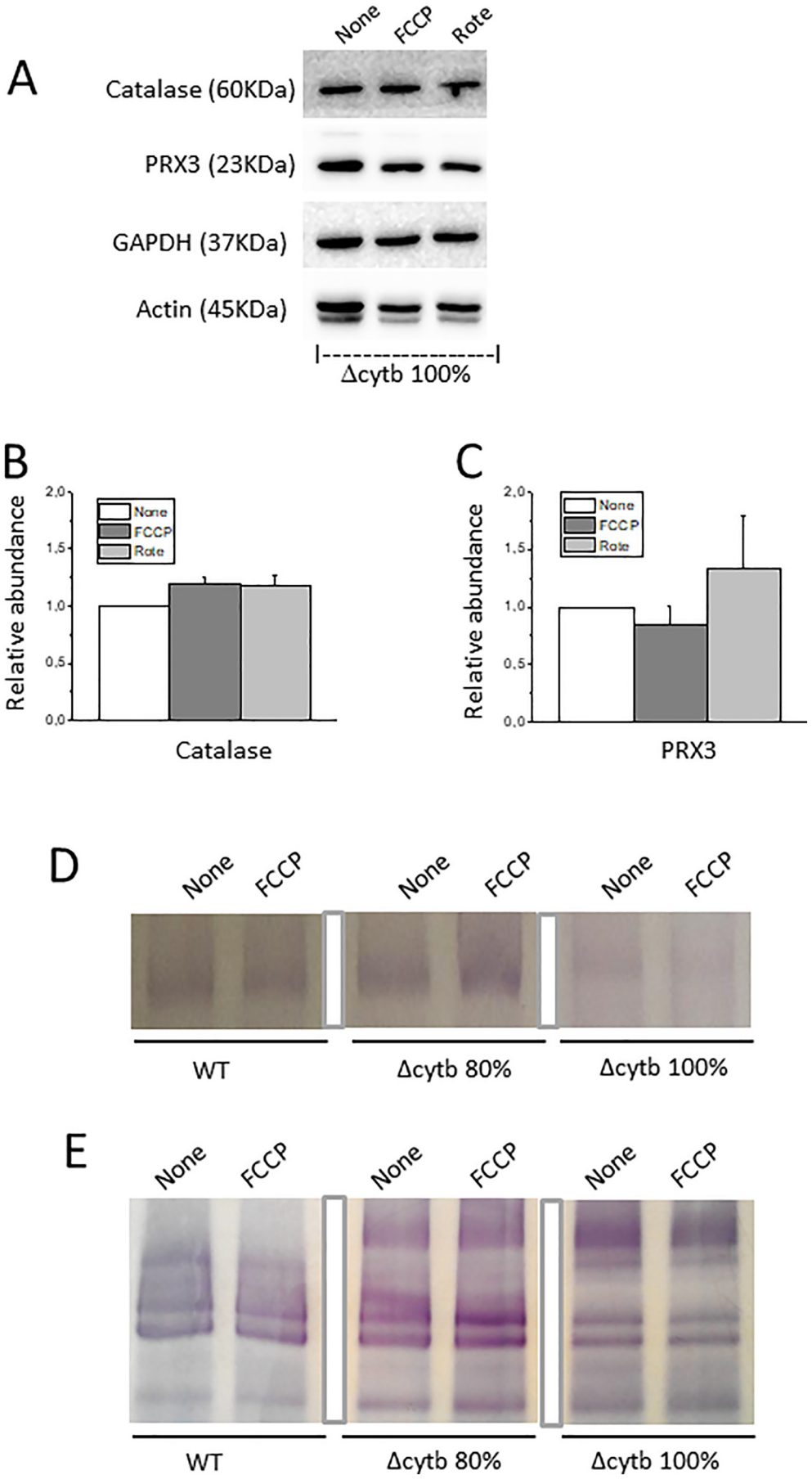

Fig. 5. Effect of FCCP and rotenone on the antioxidant enzymes and CI-IGA.
A) Δcytb 100% cybrids were untreated (none) or incubated for 24 h with 1 μM FCCP or 48 h with 500 nM Rotenone. Western blot analysis was carried out in cellular lysates, by using antibodies against catalase, peroxiredoxin 3 (PRX3), glyceraldehyde 3-P dehydrogenase (GAPDH) and actin. The blots are representative of three biological replicates in independent experiments; images of membranes were obtained after ~ 60 s of exposition. Densitometric analysis of catalase (B) and PRX3 (C) bands intensity was determined as a ratio over GAPDH; values (mean ± SD of three independent experiments) are expressed as ratio on untreated cells. D) WT, Δcytb 80% and Δcytb 100% cybrids were incubated for 24 h in the absence (none) or presence of 1 μM FCCP. The CI-IGA was determined in DDM-solubilized mitochondrial fractions or E) in digitonin-solubilized mitochondrial fractions, after separation by CN-PAGE, as described in Methods. Gels are representative of three independent experiments. The bar indicates that one lane was removed from the gel.

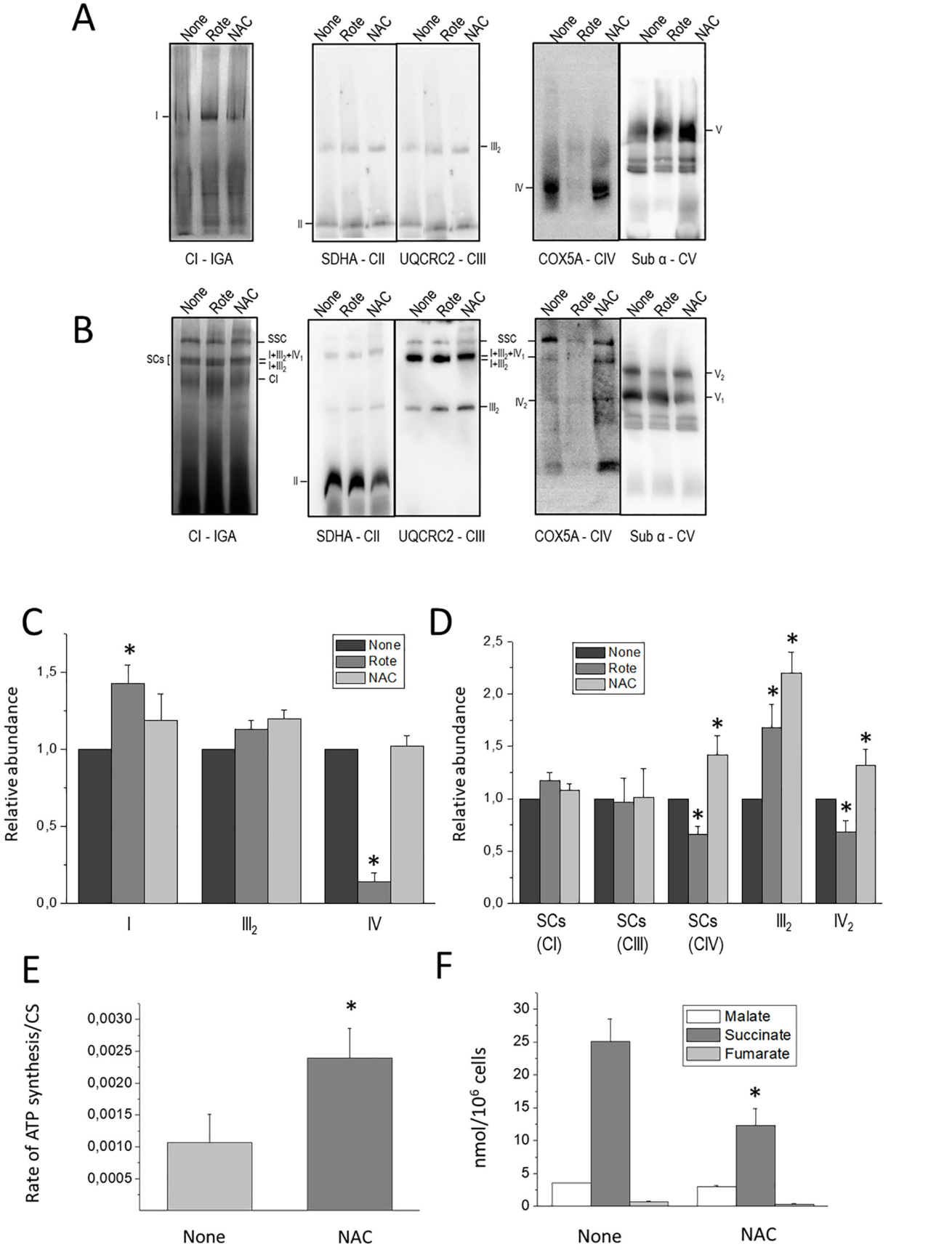

(caption on next page)

Fig. 6. Effect of rotenone and NAC on complexes content, SCs organization and bioenergetics.
Δcytb 100% cybrids were untreated (none) or incubated for 48 h with 500 nM rotenone or 72 h with 10 mM NAC, as described in Material and Methods. A) DDM-solubilized mitochondria-enriched fractions were separated by BN-PAGE; CI-IGA and western blot analysis were performed as described in Fig. 2A. Immunodetection of CII and CIII was simultaneously performed in the same membrane. Representative blots of three biological replicates in independent experiments are shown; images of membranes were obtained after ~120 s of exposition.
B) Digitonin-solubilized mitoplasts were separated by BN-PAGE, and treated exactly as described in A). Representative blots from at least three biological replicates in independent experiments are shown. The signals of the bands of indicated complexes in DDM- (C) or complexes/SCs in digitonin-solubilized (D) mitochondria were quantified by densitometry after normalization to CII, and indicated as mean ± SD. Values are expressed as a ratio of untreated cells. Statistical analysis was performed using the One sample *t*-test; * indicates $p < 0.05$ as the level of significance.
E) Δcytb 100% cybrids were untreated (none) or treated for 72 h with 10 mM NAC and the rate of ATP synthesis driven by malate + pyruvate was measured as described in Fig. 4B, in digitonin-permeabilized cells. Data are means ± SD of at least five independent experiments, and were normalized for citrate synthase activity. Statistical analysis was performed using the Two samples *t*-test; * denotes values significantly different from untreated cells: $p < 0.05$. F) The cellular content of malate, succinate and fumarate was determined by LC-ESI-MS/MS, as described in Methods. The data are mean ± SD of three independent experiments. Statistical analysis was performed using the Two samples *t*-test; * denotes values significantly different from untreated cells: $p < 0.01$.

indicate that several CI inhibitors that act at the quinone binding pocket (i.e., amilorides, acetogenins, quinazoniles, etc.) also interact with these subunits distributed around the predicted quinone channel [47]. However, we cannot rule out that, in addition to a structural stabilization effect, rotenone treatment might also induce increased CI and CIII content through additional mechanisms. In this regard, rotenone was previously reported to induce ER stress [48,49], which has recently been shown to promote through the PERK/SCAF1 axis, the assembly of the respiratory complexes and increase OXPHOS [50]. Whether this occurs also in Δcytb 100% mutant cells treated with rotenone remains to be investigated.

More interesting is the finding that the antioxidant NAC increased not only the amount of CI and $CIII_2$, but also that of CIV, leading to partial re-assembly of respirasome (Fig. 7C). This effect is mirrored by a small but significant recovery of OXPHOS capacity, and by a clear reduction of succinate levels, supporting the notion that some electron transport function was re-established. We note that the beneficial effects of NAC may not rely only on its antioxidant activity, but also on its ability to keep reduced the intracellular environment [51]. In this regard, it is known that after oxidative damage or after hypoxia and reoxygenation, specific cysteine residues in several subunits of CI and CIII were shown to be oxidized, suggesting important structural roles for these thiol groups on maintaining the stability of the respiratory complexes [15,52]. Our hypothesis is that NAC provides optimal redox conditions for respiratory complexes assembly and respirasome reorganization by promoting the reduction of specific cysteine residues that are structurally critical. In agreement with this finding, NAC has been recently described to preserve the energetic efficiency and SCs assembly in post-ischemic hearts after ischemia and reperfusion [53].

The effect of NAC is also in line with reports showing that SOD2 overexpression, or the presence of a SOD mimetic, improves SC stability in mitochondria from mouse lung fibroblasts that lack the Rieske iron-sulfur protein, highlighting the role of ROS on the modulation of SC remodeling [13]. Stabilization of high molecular weight SCs has recently been confirmed in distinct brain regions of the neuron-specific Rieske iron-sulfur KO mice after treatment with mitochondrial targeted antioxidant mitoTEMPO [54]. It is noteworthy that in these Rieske KO cells, pre-incubation with NAC was ineffective. Although the basis of this difference is unknown, it might be due to the insertion or stability of the Fe-S cluster cofactor of the Rieske protein, which uses cysteines as cofactor ligands. In any event, the mechanisms involved in the redox perturbation associated with the lack of the Rieske protein may be different from those acting in the Δcytb 100% cybrids. Importantly, this study correlated mechanistically the partial respirasome re-assembly induced by NAC with the weak but significant improvement of the energetic function, in term of both electron flux and ATP synthesis rate.

In conclusion, our study describes in detail how the respiratory complexes supramolecular organization can adapt to a severe CIII pathogenic dysfunction, maintaining preferential structural CI and CIII interaction, despite a marked decrease of CI, CIII and CIV levels.

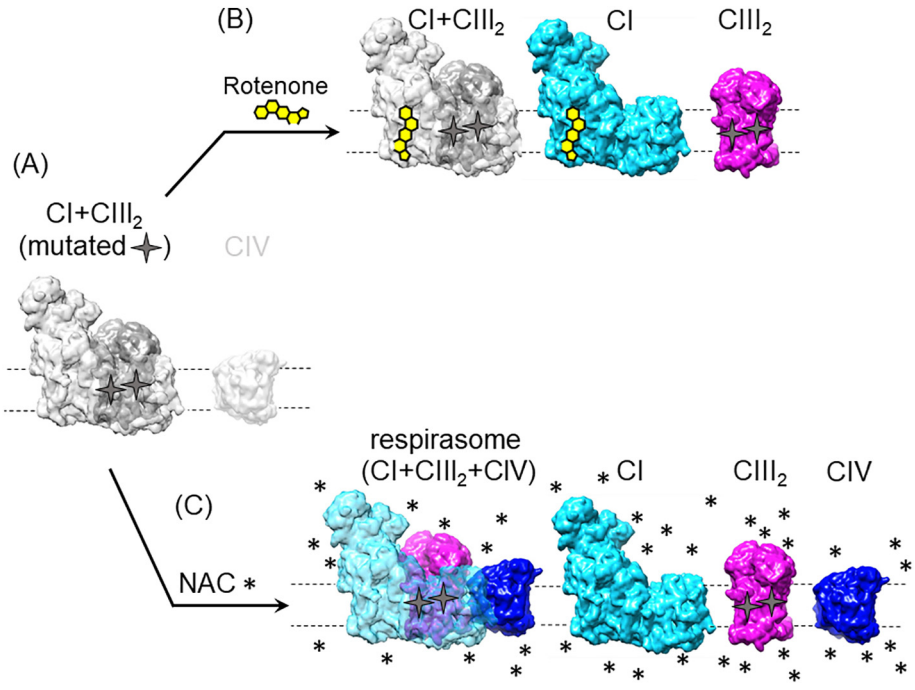

Fig. 7. Different tuning of respiratory complexes organization by rotenone and NAC.
A) In cells bearing the homoplasmic *MT-CYB* deletion, the CI, $CIII_2$ and CIV content is strongly reduced although some CI + $CIII_2$ SC is still present (in gray).
B) Pre-incubation with rotenone, stabilizes isolated CI (light blue) and $CIII_2$ (purple), but not CIV, without increasing the amount of CI + $CIII_2$ SC (gray).
C) NAC treatment stabilizes CI (light blue), $CIII_2$ (purple) and CIV (dark blue), partially re-assembling the respirasome. (For interpretation of the references to color in this figure legend, the reader is referred to the web version of this article.)

Furthermore, rotenone treatment stabilizes both isolated CI and CIII, but is unable to increase the amount of assembled CI + CIII SC. Finally, we identify NAC as a compound able to stabilize CI, CIII and CIV promoting a limited re-assembly of the respirasome. Therefore, by tuning the SCs organization NAC can improve the energetic efficiency, suggesting potential strategies that may be used to palliate multisystem symptoms associated with CIII dysfunctions.

Transparency document

The Transparency document associated with this article can be found, in online version.

Acknowledgments

This work was supported by National Institutes of Health [GM 38237 to FD and M.R], providing a fellowship to VCT, by Ministero dell' Istruzione, dell' Università e della Ricerca [PRIN grant 20107Z8XBW to M.R], and by Ministero della Salute [funding "Ricerca Corrente" to VC]. In addition, Fondazione Umberto Veronesi [CZ received a research fellowship 2019] and UBI-Banca Carime, Bari, Italy provided a financial support to M.Roberti through a fellowship to LS.

References

[1] G. Lenaz, M.L. Genova, Structure and organization of mitochondrial respiratory complexes: a new understanding of an old subject, Antioxid. Redox Signal. 12 (2010) 961–1008.
[2] T. Lobo-Jarne, C. Ugalde, Respiratory chain supercomplexes: structures, Function and Biogenesis, Semin. Cell Dev. Biol. 76 (2018) 179–190.
[3] J.A. Letts, L.A. Sazanov, Clarifying the supercomplex: the higher-order organization of the mitochondrial electron transport chain, Nat. Struct. Mol. Biol. 24 (2017) 800–808.
[4] D. Milenkovic, J.N. Blaza, N.-G. Larsson, J. Hirst, The enigma of the respiratory chain supercomplex, Cell Metab. 25 (2017) 765–776.
[5] J. Hirst, Open questions: respiratory chain supercomplexes-why are they there and what do they do? BMC Biol. 16 (2018) 111.
[6] H. Schägger, R. de Coo, M.F. Bauer, S. Hofmann, C. Godinot, U. Brandt, Significance of respirasomes for the assembly/stability of human respiratory chain complex I, J. Biol. Chem. 279 (2004) 36349–36353.
[7] E. Lamantea, F. Carrara, C. Mariotti, L. Morandi, V. Tiranti, M. Zeviani, A novel nonsense mutation (Q352X) in the mitochondrial cytochrome b gene associated with a combined deficiency of complexes I and III, Neuromuscul. Disord. NMD 12 (2002) 49–52.
[8] R. Acín-Pérez, M.P. Bayona-Bafaluy, P. Fernández-Silva, R. Moreno-Loshuertos, A. Pérez-Martos, C. Bruno, C.T. Moraes, J.A. Enríquez, Respiratory complex III is required to maintain complex I in mammalian mitochondria, Mol. Cell 13 (2004) 805–815.
[9] M. D'Aurelio, C.D. Gajewski, G. Lenaz, G. Manfredi, Respiratory chain supercomplexes set the threshold for respiration defects in human mtDNA mutant cybrids, Hum. Mol. Genet. 15 (2006) 2157–2169.
[10] Y. Li, M. D'Aurelio, J.-H. Deng, J.-S. Park, G. Manfredi, P. Hu, J. Lu, Y. Bai, An assembled complex IV maintains the stability and activity of complex I in mammalian mitochondria, J. Biol. Chem. 282 (2007) 17557–17562.
[11] H.-T. Hornig-Do, T. Tatsuta, A. Buckermann, M. Bust, G. Kollberg, A. Rötig, M. Hellmich, L. Nijtmans, R.J. Wiesner, Nonsense mutations in the COX1 subunit impair the stability of respiratory chain complexes rather than their assembly, EMBO J. 31 (2012) 1293–1307.
[12] F. Diaz, H. Fukui, S. Garcia, C.T. Moraes, Cytochrome c oxidase is required for the assembly/stability of respiratory complex I in mouse fibroblasts, Mol. Cell. Biol. 26 (2006) 4872–4881.
[13] F. Diaz, J.A. Enríquez, C.T. Moraes, Cells lacking Rieske iron-sulfur protein have a reactive oxygen species-associated decrease in respiratory complexes I and IV, Mol. Cell. Biol. 32 (2012) 415–429.
[14] E. Fernández-Vizarra, M. Zeviani, Nuclear gene mutations as the cause of mitochondrial complex III deficiency, Front. Genet. 6 (2015) 134.
[15] A. Guarás, E. Perales-Clemente, E. Calvo, R. Acín-Pérez, M. Loureiro-Lopez, C. Pujol, I. Martínez-Carrascoso, E. Nuñez, F. García-Marqués, M.A. Rodríguez-Hernández, A. Cortés, F. Diaz, A. Pérez-Martos, C.T. Moraes, P. Fernández-Silva, A. Trifunovic, P. Navas, J. Vazquez, J.A. Enríquez, The CoQH2/CoQ ratio serves as a sensor of respiratory chain efficiency, Cell Rep. 15 (2016) 197–209.
[16] R. Acín-Pérez, P. Fernández-Silva, M.L. Peleato, A. Pérez-Martos, J.A. Enriquez, Respiratory active mitochondrial supercomplexes, Mol. Cell 32 (2008) 529–539.
[17] R. Acin-Perez, J.A. Enriquez, The function of the respiratory supercomplexes: the plasticity model, Biochim. Biophys. Acta 1837 (2014) 444–450.
[18] E. Lapuente-Brun, R. Moreno-Loshuertos, R. Acín-Pérez, A. Latorre-Pellicer, C. Colás, E. Balsa, E. Perales-Clemente, P.M. Quirós, E. Calvo, M.A. Rodríguez-Hernández, P. Navas, R. Cruz, Á. Carracedo, C. López-Otín, A. Pérez-Martos, P. Fernández-Silva, E. Fernández-Vizarra, J.A. Enríquez, Supercomplex assembly determines electron flux in the mitochondrial electron transport chain, Science 340 (2013) 1567–1570.
[19] C.I. Ragan, C. Heron, The interaction between mitochondrial NADH-ubiquinone oxidoreductase and ubiquinol-cytochrome c oxidoreductase evidence for stoicheiometric association, Biochem. J. 174 (1978) 783–790.
[20] J.A. Enriquez, G. Lenaz, Coenzyme q and the respiratory chain: coenzyme q pool and mitochondrial supercomplexes, Mol. Syndromol. 5 (2014) 119–140.
[21] J.N. Blaza, R. Serreli, A.J.Y. Jones, K. Mohammed, J. Hirst, Kinetic evidence against partitioning of the ubiquinone pool and the catalytic relevance of respiratory-chain supercomplexes, Proc. Natl. Acad. Sci. U. S. A. 111 (2014) 15735–15740.
[22] J.G. Fedor, J. Hirst, Mitochondrial supercomplexes do not enhance catalysis by quinone channeling, Cell Metab., 28 e4 (2018) 525–531.
[23] J. Gu, M. Wu, R. Guo, K. Yan, J. Lei, N. Gao, M. Yang, The architecture of the mammalian respirasome, Nature 537 (2016) 639–643.
[24] R. Guo, S. Zong, M. Wu, J. Gu, M. Yang, Architecture of human mitochondrial respiratory megacomplex I2III2IV2, Cell 170 (2017) 1247-1257.e12.
[25] J.A. Letts, K. Fiedorczuk, L.A. Sazanov, The architecture of respiratory supercomplexes, Nature 537 (2016) 644–648.
[26] M. Wu, J. Gu, R. Guo, Y. Huang, M. Yang, Structure of mammalian respiratory supercomplex I1III2IV1, Cell 167 (2016) 1598-1609.e10.
[27] V. Carossa, A. Ghelli, C.V. Tropeano, M.L. Valentino, L. Iommarini, A. Maresca, L. Caporali, C. La Morgia, R. Liguori, P. Barboni, M. Carbonelli, G. Rizzo, C. Tonon, R. Lodi, A. Martinuzzi, V. De Nardo, M. Rugolo, L. Ferretti, F. Gandini, M. Pala, et al., A novel in-frame 18-bp microdeletion in MT-CYB causes a multisystem disorder with prominent exercise intolerance, Hum. Mutat. 35 (2014) 954–958.
[28] C.V. Tropeano, J. Fiori, V. Carelli, L. Caporali, F. Daldal, A.M. Ghelli, M. Rugolo, Complex II phosphorylation is triggered by unbalanced redox homeostasis in cells lacking complex III, Biochim. Biophys. Acta Bioenerg. 1859 (2018) 182–190.
[29] A. Ghelli, C.V. Tropeano, M.A. Calvaruso, A. Marchesini, L. Iommarini, A.M. Porcelli, C. Zanna, V. De Nardo, A. Martinuzzi, F. Wibrand, J. Vissing, I. Kurelac, G. Gasparre, N. Selamoglu, F. Daldal, M. Rugolo, The cytochrome b p278Y > C mutation causative of a multisystem disorder enhances superoxide production and alters supramolecular interactions of respiratory chain complexes, Hum. Mol. Genet. 22 (2013) 2141–2151.
[30] I. Wittig, M. Karas, H. Schägger, High resolution clear native electrophoresis for in-gel functional assays and fluorescence studies of membrane protein complexes, Mol. Cell. Proteomics MCP 6 (2007) 1215–1225.
[31] A.M. Porcelli, A. Angelin, A. Ghelli, E. Mariani, A. Martinuzzi, V. Carelli, V. Petronilli, P. Bernardi, M. Rugolo, Respiratory complex I dysfunction due to mitochondrial DNA mutations shifts the voltage threshold for opening of the permeability transition pore toward resting levels, J. Biol. Chem. 284 (2009) 2045–2052.
[32] F. Sasarman, E.A. Shoubridge, Radioactive labeling of mitochondrial translation products in cultured cells, Methods Mol. Biol. Clifton NJ 837 (2012) 207–217.
[33] G. Hofhaus, R.M. Shakeley, G. Attardi, Use of polarography to detect respiration defects in cell cultures, Methods Enzymol. 264 (1996) 476–483.
[34] V. Giorgio, V. Petronilli, A. Ghelli, V. Carelli, M. Rugolo, G. Lenaz, P. Bernardi, The effects of idebenone on mitochondrial bioenergetics, Biochim. Biophys. Acta 1817 (2012) 363–369.
[35] J. Fiori, E. Amadesi, F. Fanelli, C.V. Tropeano, M. Rugolo, R. Gotti, Cellular and mitochondrial determination of low molecular mass organic acids by LC-MS/MS, J. Pharm. Biomed. Anal. 150 (2018) 33–38.
[36] M. Malferrari, A. Ghelli, F. Roggiani, G. Valenti, F. Paolucci, M. Rugolo, S. Rapino, Reactive oxygen species produced by mutated mitochondrial respiratory chains of entire cells monitored using modified microelectrodes, ChemElectroChem 6 (2019) 627–633.
[37] L. Iommarini, A. Ghelli, G. Leone, C.V. Tropeano, I. Kurelac, L.B. Amato, G. Gasparre, A.M. Porcelli, Mild phenotypes and proper supercomplex assembly in human cells carrying the homoplasmic m15557G > A mutation in cytochrome b gene, Hum. Mutat. 39 (2018) 92–102.
[38] K.M. Davies, T.B. Blum, W. Kühlbrandt, Conserved in situ arrangement of complex I and III2 in mitochondrial respiratory chain supercomplexes of mammals, yeast, and plants, Proc. Natl. Acad. Sci. U. S. A. 115 (2018) 3024–3029.
[39] R. Pérez-Pérez, T. Lobo-Jarne, D. Milenkovic, A. Mourier, A. Bratic, A. García-Bartolomé, E. Fernández-Vizarra, S. Cadenas, A. Delmiro, I. García-Consuegra, J. Arenas, M.A. Martín, N.-G. Larsson, C. Ugalde, COX7A2L is a mitochondrial complex III binding protein that stabilizes the III2+IV supercomplex without affecting respirasome formation, Cell Rep. 16 (2016) 2387–2398.
[40] L. Van Haute, S.F. Pearce, C.A. Powell, A.R. D'Souza, T.J. Nicholls, M. Minczuk, Mitochondrial transcript maturation and its disorders, J. Inherit. Metab. Dis. 38 (2015) 655–680.
[41] B. Rieger, D.N. Shalaeva, A.-C. Söhnel, W. Kohl, P. Duwe, A.Y. Mulkidjanian, K.B. Busch, Lifetime imaging of GFP at CoxVIIIa reports respiratory supercomplex assembly in live cells, Sci. Rep. 7 (2017) 46055.
[42] R. Baradaran, J.M. Berrisford, G.S. Minhas, L.A. Sazanov, Crystal structure of the entire respiratory complex I, Nature 494 (2013) 443–448.
[43] L.A. Sazanov, A giant molecular proton pump: structure and mechanism of respiratory complex I, Nat. Rev. Mol. Cell Biol. 16 (2015) 375–388.
[44] V. Zickermann, C. Wirth, H. Nasiri, K. Siegmund, H. Schwalbe, C. Hunte, U. Brandt, Structural biology mechanistic insight from the crystal structure of mitochondrial complex I, Science 347 (2015) 44–49.
[45] C. Wirth, U. Brandt, C. Hunte, V. Zickermann, Structure and function of mitochondrial complex I, Biochim. Biophys. Acta 1857 (2016) 902–914.
[46] K. Fiedorczuk, J.A. Letts, G. Degliesposti, K. Kaszuba, M. Skehel, L.A. Sazanov, Atomic structure of the entire mammalian mitochondrial complex I, Nature 538

(2016) 406–410.
[47] S. Uno, H. Kimura, M. Murai, H. Miyoshi, Exploring the quinone/inhibitor-binding pocket in mitochondrial respiratory complex I by chemical biology approaches, J. Biol. Chem. 294 (2019) 679–696.
[48] Y.-Y. Chen, G. Chen, Z. Fan, J. Luo, Z.-J. Ke, GSK3β and endoplasmic reticulum stress mediate rotenone-induced death of SK-N-MC neuroblastoma cells, Biochem. Pharmacol. 76 (2008) 128–138.
[49] G. Han, R.J. Casson, G. Chidlow, J.P.M. Wood, The mitochondrial complex I inhibitor rotenone induces endoplasmic reticulum stress and activation of GSK-3β in cultured rat retinal cells, Investig. Opthalmology Vis. Sci. 55 (2014) 5616.
[50] E. Balsa, M.S. Soustek, A. Thomas, S. Cogliati, C. García-Poyatos, E. Martín-García, M. Jedrychowski, S.P. Gygi, J.A. Enriquez, P. Puigserver, ER and nutrient stress promote assembly of respiratory chain supercomplexes through the PERK-eIF2α axis, Mol. Cell 74 (2019) 877–890.
[51] K.R. Atkuri, J.J. Mantovani, L.A. Herzenberg, L.A. Herzenberg, N-Acetylcysteine-a safe antidote for cysteine/glutathione deficiency, Curr. Opin. Pharmacol. 7 (2007) 355–359.
[52] T.R. Hurd, T.A. Prime, M.E. Harbour, K.S. Lilley, M.P. Murphy, Detection of reactive oxygen species-sensitive thiol proteins by redox difference gel electrophoresis: implications for mitochondrial redox signaling, J. Biol. Chem. 282 (2007) 22040–22051.
[53] I. Ramírez-Camacho, F. Correa, M. El Hafidi, A. Silva-Palacios, M. Ostolga-Chavarría, M. Esparza-Perusquía, S. Olvera-Sánchez, O. Flores-Herrera, C. Zazueta, Cardioprotective strategies preserve the stability of respiratory chain supercomplexes and reduce oxidative stress in reperfused ischemic hearts, Free Radic. Biol. Med. 129 (2018) 407–417.
[54] M.R. Anwar, A. Saldana-Caboverde, S. Garcia, F. Diaz, The organization of mitochondrial supercomplexes is modulated by oxidative stress in vivo in mouse models of mitochondrial encephalopathy, Int. J. Mol. Sci. 19 (2018).